Optimal Uplink Pinching-Antenna Activation

Zhenqiao Cheng and Chongjun Ouyang

***Abstract*—An uplink multiuser pinching-antenna system (PASS) is considered, where multiple dielectric waveguides are deployed at the base station and one pinching antenna (PA) is activated on each waveguide. For practical implementation, each PA is restricted to a finite number of preconfigured locations. The resulting uplink sum-rate maximization problem is represented as a layered tree search. Three algorithms are then developed: a greedy search (GS), a beam search (BeS), and an optimal branch-and-bound (BnB) search. In GS, the locally best branch is selected through efficient matrix-inverse updates. In BeS, several promising partial paths are retained to provide a tunable performance-complexity tradeoff. In BnB, noncompetitive subtrees are pruned through a monotonic transformed objective without loss of optimality. Substantial gains over a conventional fixed array are demonstrated by numerical results. Near-optimal performance is also achieved by GS and moderate-width BeS at a lower computational cost than BnB.**

***Index Terms*—Antenna activation, beam search, branch-and-bound, pinching antennas, uplink sum-rate.**

I. Introduction

Flexible-antenna technologies have attracted increasing attention because antenna-location reconfiguration can reshape wireless channels [1], [2]. The pinching-antenna system (PASS) provides a recent and practical realization of this concept [3], [4]. In PASS, dielectric waveguides carry radio-frequency signals, while low-cost dielectric particles called pinching antennas (PAs) create radiating or receiving points at desired positions along the waveguides [5], [6]. A waveguide can span the service region and offer a much larger reconfigurable aperture than conventional fluid and movable arrays. PA activation at favorable propagation locations can thus reduce large-scale path loss and alleviate signal blockage, especially in high-frequency bands [5], [6].

Existing studies have explored PASS for uplink and downlink transmission and for several emerging applications; a recent overview is available in [7]. Many of these studies permit each PA to move continuously along its waveguide [8]–[10]. Continuous activation may, however, be difficult to realize because practical mechanical, magnetic, or electronic control mechanisms support only a finite number of activation positions. This hardware constraint motivates a discrete model in which each waveguide activates one PA from a predefined candidate set [6]. For example, a track parallel to the waveguide can hold dielectric particles at L preconfigured positions. A control mechanism presses the selected particle against the waveguide to create the desired PA, in a manner analogous to the keys of a player piano [11].

Z. Cheng is with the 6G Research Centre, China Telecom Beijing Research Institute, Beijing, 102209, China (e-mail: zhenqiao.cheng@engineer.com).

C. Ouyang is with the School of Electronic Engineering and Computer Science, Queen Mary University of London, London, E1 4NS, U.K. (e-mail: c.ouyang@qmul.ac.uk).

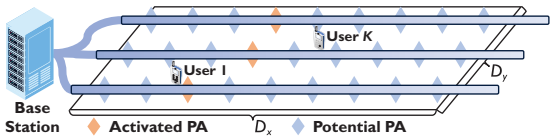

Fig. 1: Illustration of an uplink multiuser PASS.

Discrete PA activation has been studied primarily for PASS-enabled downlink transmission [11]–[15]. In contrast, uplink sum-rate maximization under discrete activation remains largely unexplored. Moreover, existing methods generally seek high-quality feasible solutions, whereas globally optimal activation and its performance benchmark have received limited attention. This article addresses these gaps for an uplink multiuser PASS. We formulate the discrete PA activation problem and recast it as a tree search. We then develop three algorithms: a low-complexity greedy search (GS), a beam search (BeS), and an optimal branch-and-bound (BnB) search. GS selects the best child at each layer and follows one path to a complete activation vector. BeS retains the best B partial paths, which reduces the risk of an unfavorable early decision and offers a tunable performance-complexity tradeoff. BnB evaluates a derived upper bound at each node and prunes any subtree that cannot improve the incumbent solution; it therefore certifies global optimality. We also characterize the computational complexity of the three algorithms. Numerical results demonstrate that discrete PA activation substantially outperforms a conventional fixed array. They further show that GS and moderate-width BeS approach the BnB benchmark at lower computational cost.

II. System Model

Consider the uplink PASS illustrated in Fig. 1, where a base station serves K single-antenna users through M dielectric waveguides. The users are located in a rectangular service region on the xy-plane. The position of user $k \in \mathcal{K} \triangleq \{1, \ldots, K\}$ is denoted by $\mathbf{u}_k = [x_k, y_k, 0]^\mathsf{T}$.

The M waveguides are deployed along the x-axis at height h and are arranged along the y-axis with spacing d. The mth waveguide has a feed point at $\boldsymbol{\psi}_0^m = [\psi_\mathrm{w}, \psi_0^m, h]^\mathsf{T}$. One PA is activated on each waveguide for uplink reception [16]–[18]. For practical activation, the PA on each waveguide can be placed only at one of L preconfigured positions collected in $\mathcal{L} \triangleq \{\psi_1, \ldots, \psi_L\}$ with $\psi_\mathrm{w} \le \psi_1 \le \ldots \le \psi_L$. If the ℓ_mth candidate is selected on waveguide m, the PA location is $\boldsymbol{\psi}_{\ell_m}^m = [\psi_{\ell_m}, \psi_0^m, h]^\mathsf{T}$ for $\ell_m \in \mathcal{L}_\mathrm{id} \triangleq \{1, \ldots, L\}$. The activation vector is defined as $\boldsymbol{\ell} = [\ell_1, \ldots, \ell_M]^\mathsf{T}$.

PASS is envisioned for operation in high-frequency bands [3], where line-of-sight (LoS) propagation dominates [19], [20]. A free-space LoS channel model is therefore adopted.

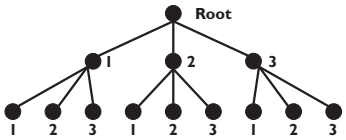

Fig. 2: Illustration of a search tree for $M = 2$ and $L = 3$.

Under this model, the spatial channel coefficient from user k to the ℓth candidate on waveguide m is modeled as [19], [20]

$$h_{\mathrm{o}}(\mathbf{u}_k, \boldsymbol{\psi}_\ell^m) = \frac{\eta^{\frac{1}{2}} \mathrm{e}^{-\mathrm{j}k_0\|\mathbf{u}_k - \boldsymbol{\psi}_\ell^m\|}}{\|\mathbf{u}_k - \boldsymbol{\psi}_\ell^m\|}, \tag{1}$$

where $\eta \triangleq \frac{c^2}{16\pi^2 f_{\mathrm{c}}^2}$, c is the speed of light, f_{c} is the carrier frequency, λ is the free-space wavelength, and $k_0 = \frac{2\pi}{\lambda}$ is the wavenumber. The in-waveguide propagation coefficient from the activated PA to the feed point is modeled as [21]

$$h_{\mathrm{i}}(\boldsymbol{\psi}_\ell^m, \boldsymbol{\psi}_0^m) = 10^{-\frac{\kappa}{20}\|\boldsymbol{\psi}_\ell^m - \boldsymbol{\psi}_0^m\|} \mathrm{e}^{-\mathrm{j}\frac{2\pi\|\boldsymbol{\psi}_\ell^m - \boldsymbol{\psi}_0^m\|}{\lambda_{\mathrm{g}}}}, \tag{2}$$

where $\lambda_{\mathrm{g}} = \frac{\lambda}{n_{\mathrm{eff}}}$ is the guided wavelength and n_{eff} is the effective refractive index of the dielectric waveguide [21]. The parameter κ denotes the average attenuation factor along the waveguide in dB/m [22]. As a result, the end-to-end channel from user k to the PA activated at waveguide m is

$$g_{m,k}(\ell) = h_{\mathrm{i}}(\boldsymbol{\psi}_\ell^m, \boldsymbol{\psi}_0^m) h_{\mathrm{o}}(\mathbf{u}_k, \boldsymbol{\psi}_\ell^m). \tag{3}$$

Let $x_k = \sqrt{P_k} s_k$ denote the transmitted signal of user k, where P_k is the transmit power and $s_k \sim \mathcal{CN}(0,1)$. The received signal at the base station can be written as follows:

$$\mathbf{y} = \mathbf{G}(\boldsymbol{\ell}) \mathbf{P}^{\frac{1}{2}} \mathbf{s} + \mathbf{n}, \tag{4}$$

where $\mathbf{P} = \mathrm{diag}(P_1, \ldots, P_K)$, $\mathbf{s} = [s_1, \ldots, s_K]^{\mathsf{T}}$, $\mathbf{G}(\boldsymbol{\ell}) \in \mathbb{C}^{M \times K}$ has entry $[\mathbf{G}(\boldsymbol{\ell})]_{m,k} = g_{m,k}(\ell_m)$, and $\mathbf{n} \sim \mathcal{CN}(\mathbf{0}, \sigma^2 \mathbf{I}_M)$ is the additive noise with covariance matrix $\sigma^2 \mathbf{I}_M$. Define $\mathbf{H}(\boldsymbol{\ell}) = \frac{1}{\sigma} \mathbf{G}(\boldsymbol{\ell}) \mathbf{P}^{\frac{1}{2}}$. Then the uplink sum-rate with optimal multiuser decoding is given by [23]

$$\mathcal{R}(\boldsymbol{\ell}) = \log_2 \det(\mathbf{I}_M + \mathbf{H}(\boldsymbol{\ell}) \mathbf{H}^{\mathsf{H}}(\boldsymbol{\ell})) \tag{5}$$

$$= \log_2 \det(\mathbf{I}_K + \mathbf{H}^{\mathsf{H}}(\boldsymbol{\ell}) \mathbf{H}(\boldsymbol{\ell})). \tag{6}$$

The PA activation problem is formulated as

$$\max_{\boldsymbol{\ell}} \quad \log_2 \det(\mathbf{I}_K + \mathbf{H}^{\mathsf{H}}(\boldsymbol{\ell}) \mathbf{H}(\boldsymbol{\ell})) \tag{7}$$

$$\text{s.t.} \quad \ell_m \in \mathcal{L}_{\mathrm{id}}, \quad m = 1, \ldots, M.$$

Problem (7) has L^M feasible activation vectors. It is therefore expensive to solve through exhaustive search when M or L is large. For clarity, define the candidate row vector

$$\mathbf{h}_{m,\ell}^{\mathsf{H}} = \frac{1}{\sigma} [g_{m,1}(\ell)\sqrt{P_1}, \ldots, g_{m,K}(\ell)\sqrt{P_K}]. \tag{8}$$

Selecting $\boldsymbol{\ell}$ is equivalent to selecting one row from each set

$$\mathcal{S}_m = \{\mathbf{h}_{m,1}^{\mathsf{H}}, \ldots, \mathbf{h}_{m,L}^{\mathsf{H}}\}. \tag{9}$$

Thus, (7) is a sub-array selection problem with M sub-arrays and L candidates per sub-array.

III. Tree-Search Based Activation

A. Search Tree and Rate Recursion

Problem (7) can be represented by an M-layer search tree, as exemplified in Fig. 2. The root node has no activated PA. The mth layer corresponds to waveguide m, and each node in this layer is labeled by one candidate index $\ell_m \in \mathcal{L}_{\mathrm{id}}$. Hence, a path from the root to a leaf node is an activation vector $\boldsymbol{\ell} = [\ell_1, \ldots, \ell_M]^{\mathsf{T}}$.

For a partial path $\boldsymbol{\ell}_{1:n} = [\ell_1, \ldots, \ell_n]^{\mathsf{T}}$, let $\mathbf{H}_n \in \mathbb{C}^{n \times K}$ denote the effective channel matrix formed by the first n selected rows. Its partial sum-rate is given by

$$\mathcal{R}_n = \log_2 \det(\mathbf{I}_K + \mathbf{H}_n^{\mathsf{H}} \mathbf{H}_n), \quad \mathcal{R}_0 = 0. \tag{10}$$

Suppose that the candidate ℓ on waveguide $m = n+1$ is appended to the current path. By Sylvester's determinant identity, we obtain

$$\mathcal{R}_{n+1} = \log_2 \det(\mathbf{I}_K + \mathbf{H}_n^{\mathsf{H}} \mathbf{H}_n + \mathbf{h}_{m,\ell} \mathbf{h}_{m,\ell}^{\mathsf{H}}) \tag{11}$$

$$= \mathcal{R}_n + \log_2(1 + \mathbf{h}_{m,\ell}^{\mathsf{H}} \mathbf{G}_n \mathbf{h}_{m,\ell}), \tag{12}$$

where $\mathbf{G}_n = (\mathbf{I}_K + \mathbf{H}_n^{\mathsf{H}} \mathbf{H}_n)^{-1}$. The incremental rate of this branch is given by

$$\Delta_{m,\ell,n} = \log_2(1 + \mathbf{h}_{m,\ell}^{\mathsf{H}} \mathbf{G}_n \mathbf{h}_{m,\ell}). \tag{13}$$

Therefore, a node can be evaluated from its parent by one quadratic form. After the branch $\ell^\star$ is selected on waveguide m, the inverse matrix is updated via the Sherman–Morrison formula [24] as

$$\mathbf{G}_{n+1} = \mathbf{G}_n - \frac{\mathbf{G}_n \mathbf{h}_{m,\ell^\star} \mathbf{h}_{m,\ell^\star}^{\mathsf{H}} \mathbf{G}_n}{1 + \mathbf{h}_{m,\ell^\star}^{\mathsf{H}} \mathbf{G}_n \mathbf{h}_{m,\ell^\star}}. \tag{14}$$

This recursion avoids a fresh matrix inversion at each visited node [25].

Algorithm 1 Greedy PA Activation

1: Initialize $\boldsymbol{\ell} = \mathbf{0}$, $\mathbf{G}_0 = \mathbf{I}_K$, and $\mathcal{R}_0 = 0$.
2: **for** $m = 1, \ldots, M$ **do**
3: Compute $\Delta_{m,\ell,m-1}$ in (13) for all $\ell \in \mathcal{L}_{\mathrm{id}}$.
4: Set $\ell_m = \mathrm{argmax}_{\ell \in \mathcal{L}_{\mathrm{id}}} \Delta_{m,\ell,m-1}$.
5: Update $\mathcal{R}_m = \mathcal{R}_{m-1} + \Delta_{m,\ell_m,m-1}$.
6: Update $\mathbf{G}_m$ using (14).
7: **end for**
8: Output $\boldsymbol{\ell}$ and $\mathcal{R}_M$.

B. Greedy Activation

Greedy activation is the simplest way to traverse the tree. At each layer, it keeps only one survivor path, namely the path with the largest immediate rate increase. Its intuition is that (13) measures the new spatial dimension contributed by a candidate PA after the already selected waveguides have been accounted for through $\mathbf{G}_n$. A candidate with large $\Delta_{m,\ell,n}$ either has a strong channel norm or contributes a direction that is weakly represented by previous selections. Thus, the greedy rule selects the most useful PA location for the current residual channel. The complete GS procedure is summarized in Algorithm 1.

The greedy method is not guaranteed to be optimal because a locally strong candidate may limit the choices of later waveguides. Nevertheless, it has two important roles. First, it gives a very low-complexity activation rule. Second, it provides a good initial complete path for the BnB algorithm, which helps tighten the pruning threshold.

Algorithm 2 Beam Search for PA Activation

Initialize the path list $\mathcal{P}_0 = \{(\emptyset, \mathbf{I}_K, 0)\}$.
for $m = 1, \ldots, M$ **do**
  Set $\mathcal{C} = \emptyset$.
  for each path $(\boldsymbol{\ell}_{1:m-1}, \mathbf{G}_{m-1}, \mathcal{R}_{m-1}) \in \mathcal{P}_{m-1}$ **do**
    for $\ell = 1, \ldots, L$ **do**
      Compute $\Delta_{m,\ell,m-1}$ by the path-specific $\mathbf{G}_{m-1}$.
      Form $\boldsymbol{\ell}_{1:m} = [\boldsymbol{\ell}_{1:m-1}^{\mathsf{T}}, \ell]^{\mathsf{T}}$.
      Set $\mathcal{R}_m = \mathcal{R}_{m-1} + \Delta_{m,\ell,m-1}$.
      Update $\mathbf{G}_m$ using (14).
      Add $(\boldsymbol{\ell}_{1:m}, \mathbf{G}_m, \mathcal{R}_m)$ to $\mathcal{C}$.
    end for
  end for
  Keep the $\min\{B, |\mathcal{C}|\}$ entries in $\mathcal{C}$ with the largest $\mathcal{R}_m$ and store them in $\mathcal{P}_m$.
end for
Output the complete path in $\mathcal{P}_M$ with the largest $\mathcal{R}_M$.

C. Beam Search Activation

The greedy search may discard a partial path too early. To reduce this risk, BeS keeps the best B partial paths after each layer, where B is termed the beam width. Instead of following only one strongest branch, BeS maintains a beam of promising paths. At layer m, all surviving paths from layer $m-1$ are expanded by the L candidate locations of waveguide m. The partial rate of each child is computed by (13), and only the best B children are retained. The complete BeS procedure is summarized in Algorithm 2.

The beam width controls the tradeoff between performance and complexity. For $B = 1$, BeS reduces to GS. If $B \geq L^{M-1}$, no partial path is removed before the final layer and BeS is equivalent to exhaustive search. A moderate B protects near-best paths from premature removal while it keeps the number of survivors bounded.

D. Optimal Branch-and-Bound Activation

BeS is heuristic because it may delete the optimal path when that path falls outside the beam. BnB avoids this issue. It searches the same tree but prunes only when a mathematical bound proves that a partial path cannot outperform the best complete path found so far [26]. Thus, BnB provides the optimal benchmark for the proposed activation problem. The key is to construct an upper bound on the final rate reachable from a partial path. Since $\mathcal{R}_n$ is nondecreasing with n, it cannot be used directly for pruning a maximization problem. We propose to subtract from each layer an upper bound on its possible rate increment [27]–[30]. This converts the objective into a nonincreasing metric along every root-to-leaf path.

For waveguide m, define

$$\zeta_m \triangleq \max_{\ell \in \mathcal{L}_{\mathrm{id}}} \|\mathbf{h}_{m,\ell}\|_2^2, \quad Z_m \triangleq \log_2(1+\zeta_m). \tag{15}$$

Here, Z_m is a branch-independent upper bound on the rate increment that any candidate on waveguide m can contribute. This bound is simple to compute before the tree search starts. For a partial path of length n, define

$$\widetilde{\mathcal{R}}_n = \mathcal{R}_n - \sum_{m=1}^{n} Z_m. \tag{16}$$

The following lemma establishes the required monotonicity.

Lemma 1. *For any partial path and any candidate ℓ on waveguide $n+1$, the transformed objective satisfies*

$$\widetilde{\mathcal{R}}_{n+1} \leq \widetilde{\mathcal{R}}_n. \tag{17}$$

Proof: Since $\mathbf{G}_n = (\mathbf{I}_K + \mathbf{H}_n^{\mathsf{H}}\mathbf{H}_n)^{-1}$, we have $\mathbf{0} \preceq \mathbf{G}_n \preceq \mathbf{I}_K$ [24]. Hence,

$$\mathbf{h}_{n+1,\ell}^{\mathsf{H}} \mathbf{G}_n \mathbf{h}_{n+1,\ell} \leq \|\mathbf{h}_{n+1,\ell}\|_2^2 \leq \zeta_{n+1}. \tag{18}$$

It follows from (13) that

$$\Delta_{n+1,\ell,n} \leq \log_2(1+\zeta_{n+1}) = Z_{n+1}. \tag{19}$$

Using (16), we obtain

$$\widetilde{\mathcal{R}}_{n+1} = \widetilde{\mathcal{R}}_n + \Delta_{n+1,\ell,n} - Z_{n+1} \leq \widetilde{\mathcal{R}}_n. \tag{20}$$

This completes the proof. ∎

At the final layer, the offset $\sum_{m=1}^{M} Z_m$ is fixed for all complete activation vectors. Therefore,

$$\mathrm{argmax}_{\boldsymbol{\ell}}\, \mathcal{R}_M(\boldsymbol{\ell}) = \mathrm{argmax}_{\boldsymbol{\ell}}\, \widetilde{\mathcal{R}}_M(\boldsymbol{\ell}). \tag{21}$$

The transformed objective can thus be used for pruning without changing the optimal solution. Let Γ denote the best transformed objective among all complete paths visited so far. If a partial path satisfies $\widetilde{\mathcal{R}}_n \leq \Gamma$, all of its descendants can be pruned because the lemma guarantees that no descendant can exceed $\widetilde{\mathcal{R}}_n$. Equivalently, the descendant rate satisfies

$$\mathcal{R}_M \leq \widetilde{\mathcal{R}}_n + \sum_{m=1}^{M} Z_m, \tag{22}$$

which cannot beat the current best complete solution when $\widetilde{\mathcal{R}}_n \leq \Gamma$. The GS solution initializes Γ, so a stronger initial incumbent permits more pruning. The complete depth-first BnB search is summarized in Algorithm 3.

E. Complexity Discussion

The search tree has L^M leaf nodes and $\frac{L^{M+1}-1}{L-1}$ total nodes. Exhaustive search evaluates all leaves. If each leaf recomputes the log-determinant from scratch, the complexity increases exponentially with M. With the recursion in (13) and (14), each visited child node requires one quadratic form and one rank-one update, whose dominant cost is $\mathcal{O}(K^2)$.

GS visits ML child nodes and stores one path, so its complexity is $\mathcal{O}(MLK^2)$ and its memory cost is $\mathcal{O}(K^2)$. BeS visits at most L nodes in the first layer and BL nodes in each later layer. Its complexity is therefore $\mathcal{O}(MBLK^2)$, and its memory cost is $\mathcal{O}(BK^2)$ because each surviving path stores its own inverse matrix. BnB has the same worst-case order as exhaustive search because the bound may fail to prune in the worst case. In practice, its complexity is proportional to the number of visited nodes N_{vis}, i.e., $\mathcal{O}(N_{\mathrm{vis}}K^2)$. The value of N_{vis} is often much smaller than the full tree size when the GS initialization is strong and the offset bound is tight.

IV. Numerical Results

Unless otherwise specified, we set $M = K = 4$, $f_{\mathrm{c}} = 28$ GHz, $n_{\mathrm{eff}} = 1.4$, $\kappa = 0.08$ dB/m, $h = 3$ m, $P_1 =$

Algorithm 3 Branch-and-Bound PA Activation

Compute ζ_m and Z_m for $m = 1, \ldots, M$.
Run Algorithm 1 to obtain an initial complete path $\boldsymbol{\ell}^{\mathrm{g}}$.
Set $\Gamma = \mathcal{R}(\boldsymbol{\ell}^{\mathrm{g}}) - \sum_{m=1}^{M} Z_m$ and $\boldsymbol{\ell}^{\star} = \boldsymbol{\ell}^{\mathrm{g}}$.
Start from the root node with $n = 0$, $\mathbf{G}_0 = \mathbf{I}_K$, $\mathcal{R}_0 = 0$, and $\widetilde{\mathcal{R}}_0 = 0$.
Visit child nodes in descending order of $\Delta_{n+1,\ell,n}$.
if a visited node has depth $n < M$ **then**
  Compute $\widetilde{\mathcal{R}}_n = \mathcal{R}_n - \sum_{m=1}^{n} Z_m$.
  if $\widetilde{\mathcal{R}}_n \leq \Gamma$ **then**
    Prune this node and all its descendants.
  else
    Branch to the next layer after updating $\mathbf{G}_n$ by (14).
  end if
else
  Compute $\widetilde{\mathcal{R}}_M = \mathcal{R}_M - \sum_{m=1}^{M} Z_m$.
  if $\widetilde{\mathcal{R}}_M > \Gamma$ **then**
    Set $\Gamma = \widetilde{\mathcal{R}}_M$ and update $\boldsymbol{\ell}^{\star}$.
  end if
end if
Continue until all non-pruned nodes have been visited.
Output $\boldsymbol{\ell}^{\star}$.

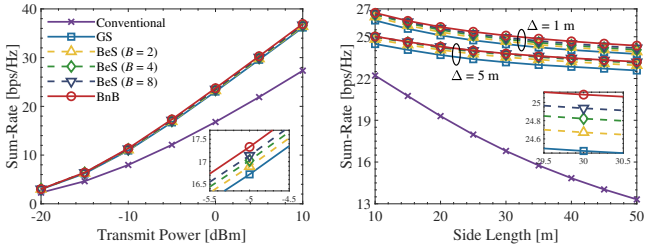

(a) $\mathcal{R}(\boldsymbol{\ell})$ versus P. (b) $\mathcal{R}(\boldsymbol{\ell})$ versus D_x.

Fig. 3: Sum-rate comparison.

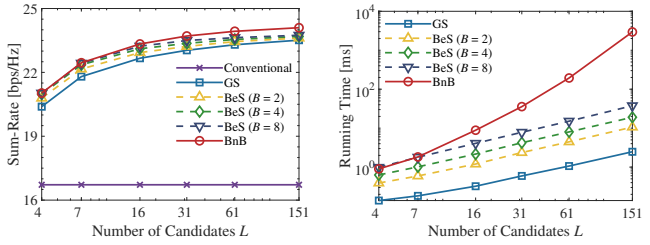

(a) Sum-rate. (b) Running time.

Fig. 4: Impact of the number of candidates.

$\ldots = P_K = P = 0$ dBm, and $\sigma^2 = -90$ dBm. The users are independently and uniformly distributed over a $D_x \times D_y$ ground region with $D_x = 30$ m and $D_y = 10$ m. The waveguides span $[0, D_x]$ along the x-axis, and their y-coordinates are $\psi_0^m = -\frac{D_y}{2} + \frac{D_y(m-1)}{M-1}$. All feed points have $\psi_{\mathrm{w}} = 0$. The L candidate locations uniformly cover each waveguide with spacing $\Delta = \frac{D_x}{L-1}$. The conventional benchmark is a centered M-element array parallel to the y-axis with half-wavelength spacing. All results are averaged over 1000 independent user deployments. The simulations use MathWorks MATLAB R2020b on a computer with a 2.60-GHz Intel Core i5-13500H CPU and 32 GB RAM.

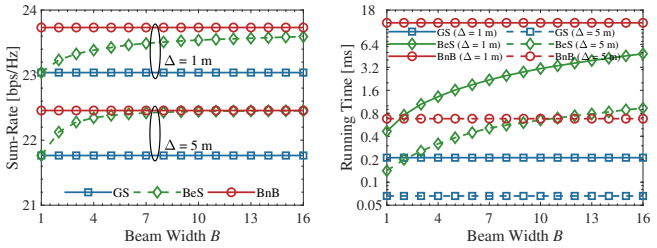

(a) Sum-rate. (b) Running time.

Fig. 5: Impact of beam width.

Fig. 3 compares the achievable sum-rates. PASS consistently outperforms the centered conventional array because PA activation adapts the receive locations to the user geometry. GS is already close to BnB, and BeS progressively closes the remaining gap as B increases. Fig. 3(b) further shows that the PASS advantage becomes more pronounced for a larger D_x. The conventional array suffers a substantial free-space path-loss penalty as the service region expands. PASS also experiences greater free-space and in-waveguide losses, but flexible PA activation offsets much of this degradation. A smaller Δ provides more candidate locations and yields an additional sum-rate gain.

Fig. 4 examines the effect of L. The sum-rate improves with the candidate-set density, while the fixed-array rate remains unchanged. Even with only $L = 4$ candidates, BnB achieves 21 bps/Hz, which is about 87% of its 24 bps/Hz value at $L = 151$ and exceeds the fixed-array rate of 17 bps/Hz. This result shows that a modest number of activation points already captures most of the PASS gain. The corresponding running times in Fig. 4(b) increase with L. The growth is most pronounced for BnB because its worst-case search space is exponential in the number of waveguides.

Fig. 5 illustrates the performance-complexity tradeoff controlled by B. GS and BnB are independent of B, whereas BeS approaches BnB as its beam widens. BeS reaches at least 99% of the BnB sum-rate at $B = 8$ for $\Delta = 1$ m and at $B = 3$ for $\Delta = 5$ m; GS remains within about 3% of BnB in both cases. A wider beam increases the BeS running time because more partial paths survive. For $\Delta = 5$ m, a sufficiently wide BeS can even be slower than BnB because the latter prunes noncompetitive subtrees. Overall, moderate values of L and B provide an attractive balance between sum-rate and computational cost.

V. Conclusion

We investigated discrete PA activation for uplink multiuser PASS through a layered tree search. We developed GS, BeS, and BnB to provide a low-complexity solution, a tunable performance-complexity tradeoff, and global optimality, respectively. Numerical results demonstrated substantial gains over a conventional fixed array. They also showed that GS and moderate-width BeS approached BnB at lower computational cost.

REFERENCES

[1] K.-K. Wong, A. Shojaeifard, K.-F. Tong, and Y. Zhang, "Fluid antenna systems," *IEEE Trans. Wireless Commun.*, vol. 20, no. 3, pp. 1950–1962, Mar. 2021.

[2] L. Zhu, W. Ma, and R. Zhang, "Movable antennas for wireless communication: Opportunities and challenges," *IEEE Commun. Mag.*, vol. 62, no. 6, pp. 114–120, Jun. 2024.

[3] A. Fukuda, H. Yamamoto, H. Okazaki, Y. Suzuki, and K. Kawai, "Pinching antenna: Using a dielectric waveguide as an antenna," *NTT DOCOMO Technical J.*, vol. 23, no. 3, pp. 5–12, Jan. 2022.

[4] Z. Ding, R. Schober, and H. V. Poor, "Flexible-antenna systems: A pinching-antenna perspective," *IEEE Trans. Commun.*, vol. 73, no. 10, pp. 9236–9253, Oct. 2025.

[5] Y. Liu, Z. Wang, X. Mu, C. Ouyang, X. Xu, and Z. Ding, "Pinching-antenna systems: Architecture designs, opportunities, and outlook," *IEEE Commun. Mag.*, vol. 64, no. 1, pp. 190–196, Jan. 2026.

[6] Y. Liu, H. Jiang, X. Xu, Z. Wang, J. Guo, C. Ouyang, X. Mu, Z. Ding, A. Nallanathan, G. K. Karagiannidis *et al.*, "Pinching-antenna systems (PASS): A tutorial," *IEEE Trans. Commun.*, vol. 74, pp. 4881–4918, 2026.

[7] Y. Liu, H. Jiang, X. Gan, X. Xu, J. Guo, Z. Wang, C. Ouyang, X. Mu, Z. Ding, A. Nallanathan *et al.*, "A survey of pinching-antenna systems (PASS)," *arXiv preprint arXiv:2601.18927*, 2026.

[8] Y. Xu, Z. Ding, and G. K. Karagiannidis, "Rate maximization for downlink pinching-antenna systems," *IEEE Wireless Commun. Lett.*, vol. 14, no. 5, pp. 1431–1435, May 2025.

[9] C. Ouyang, Z. Wang, Y. Liu, and Z. Ding, "Array gain for pinching-antenna systems (PASS)," *IEEE Commun. Lett.*, vol. 29, no. 6, pp. 1471–1475, Jun. 2025.

[10] S. A. Tegos, P. D. Diamantoulakis, Z. Ding, and G. K. Karagiannidis, "Minimum data rate maximization for uplink pinching-antenna systems," *IEEE Wireless Commun. Lett.*, vol. 14, no. 5, pp. 1516–1520, May 2025.

[11] K. Wang, Z. Ding, and R. Schober, "Antenna activation for noma assisted pinching-antenna systems," *IEEE Wireless Commun. Lett.*, vol. 14, no. 5, pp. 1526–1530, May 2025.

[12] Z. Wang, C. Ouyang, X. Mu, Y. Liu, and Z. Ding, "Modeling and beamforming optimization for pinching-antenna systems," *IEEE Trans. Commun.*, vol. 73, no. 12, pp. 13 904–13 919, Dec. 2025.

[13] X. Xu, X. Mu, Z. Wang, Y. Liu, and A. Nallanathan, "Pinching-antenna systems (PASS): Power radiation model and optimal beamforming design," *IEEE Trans. Commun.*, vol. 74, pp. 2160–2175, 2026.

[14] L. Cao, H. Yin, X. Pei, R. Song, and Y. Liu, "Multi-pin and movable-pin enabled discretely-activated pinching antenna systems," *IEEE Wireless Commun. Lett.*, vol. 15, pp. 590–594, 2026.

[15] K. Chen, C. Qi, O. A. Dobre, and C. Yuen, "Hybrid pinching antenna systems: Architecture and beamforming design," *IEEE Trans. Wireless Commun.*, vol. 25, pp. 12 129–12 144, 2026.

[16] M. Zeng, X. Li, J. Wang, G. Huang, O. A. Dobre, and Z. Ding, "Energy-efficient resource allocation for NOMA-assisted uplink pinching-antenna systems," *IEEE Wireless Commun. Lett.*, vol. 14, no. 11, pp. 3695–3699, Nov. 2025.

[17] M. Zeng, J. Wang, X. Li, G. Wang, O. A. Dobre, and Z. Ding, "Sum rate maximization for NOMA-assisted uplink pinching-antenna systems," *IEEE Wireless Commun. Lett.*, vol. 15, pp. 280 – 284, 2026.

[18] C. Ouyang, H. Jiang, Z. Wang, Y. Liu, and Z. Ding, "Uplink and downlink communications in segmented waveguide-enabled pinching-antenna systems (SWANs)," *IEEE Trans. Commun.*, vol. 74, pp. 3688–3703, 2026.

[19] Y. Liu, Z. Wang, J. Xu, C. Ouyang, X. Mu, and R. Schober, "Near-field communications: A tutorial review," *IEEE Open J. Commun. Soc.*, vol. 4, pp. 1999–2049, 2023.

[20] C. Ouyang, Z. Wang, Y. Chen, X. Mu, and P. Zhu, "A primer on near-field communications for next-generation multiple access," *Proc. IEEE*, vol. 112, no. 9, pp. 1527–1565, Sep. 2024.

[21] D. M. Pozar, *Microwave Engineering: Theory and Techniques*. Hoboken, NJ, USA: Wiley, 2021.

[22] C. Yeh and F. I. Shimabukuro, *The Essence of Dielectric Waveguides*. New York, NY, USA: Springer, 2008.

[23] R. W. Heath Jr and A. Lozano, *Foundations of MIMO Communication*. Cambridge, U.K.: Cambridge Univ. Press, 2018.

[24] R. A. Horn and C. R. Johnson, *Matrix Analysis*. New York, NY, USA: Cambridge Univ. Press, 2012.

[25] M. Gharavi-Alkhansari and A. B. Gershman, "Fast antenna subset selection in MIMO systems," *IEEE Trans. Signal Process.*, vol. 52, no. 2, pp. 339–347, Feb. 2004.

[26] Narendra and Fukunaga, "A branch and bound algorithm for feature subset selection," *IEEE Trans. Comput.*, vol. C-26, no. 9, pp. 917–922, Sep. 1977.

[27] Y. Gao, H. Vinck, and T. Kaiser, "Massive MIMO antenna selection: Switching architectures, capacity bounds, and optimal antenna selection algorithms," *IEEE Trans. Signal Process.*, vol. 66, no. 5, pp. 1346–1360, Mar. 2018.

[28] C. Ouyang, Z. Ou, L. Zhang, and H. Yang, "Optimal transmit antenna selection algorithm in massive MIMOME channels," in *Proc. IEEE Wireless Commun. Netw. Conf. (WCNC)*, 2019, pp. 1–6.

[29] Z. Cheng, N. Li, J. Zhu, X. She, C. Ouyang, and P. Chen, "Secure line-of-sight communications: Optimal antenna selection and beamforming design," in *Proc. IEEE Military Commun. Conf. (MILCOM)*, 2023, pp. 593–598.

[30] Z. Cheng, N. Li, J. Zhu, S. Yang, C. Ouyang, and X. Zhang, "Exploiting movable antennas in multicast communications," in *Proc. IEEE Global Commun. Conf. (GLOBECOM)*, 2025, pp. 2366–2371.